Monthly Notices of the ROYAL ASTRONOMICAL SOCIETY

MNRAS **520,** L16–L20 (2023) https://doi.org/10.1093/mnrasl/slac166
Advance Access publication 2023 January 2

Interpreting ALMA non-detections of *JWST* super-early galaxies

M. Kohandel ,★ A. Ferrara, A. Pallottini , L. Vallini , L. Sommovigo and F. Ziparo
Scuola Normale Superiore, Piazza dei Cavalieri 7, I-56126 Pisa, Italy

Accepted 2022 December 21. Received 2022 December 20; in original form 2022 December 6

ABSTRACT

Recent attempts to detect [O III] 88 μm emission from super-early ($z > 10$) galaxy candidates observed by *JWST* have been unsuccessful. Non-detections can be either due to wrong photometric redshifts or to the faintness of the line in such early systems. By using zoom-in simulations, we show that if redshifts of these galaxies are confirmed, they are faint and mostly fall below the local metal-poor [O III] − SFR relation as a result of their low ionization parameter, $U_{\rm ion} \lesssim 10^{-3}$. Such low $U_{\rm ion}$ values are found in galaxies that are in an early assembly stage, and whose stars are still embedded in high-density natal clouds. However, the most luminous galaxy in our sample ($\log[{\rm L}_{[{\rm O\,III}]}/{\rm L}_\odot] = 8.4$, $U_{\rm ion} \approx 0.1$) could be detected by ALMA in only 2.8 h.

Key words: methods: numerical – galaxies: evolution – galaxies: formation – galaxies: high-redshift – galaxies: ISM – infrared: general.

1 INTRODUCTION

Early observations by the *JWST* have discovered several bright (∼60 at $M_{\rm UV} \sim -21$) galaxy candidates at unprecedentedly high redshifts ($z > 10$: Adams et al. 2022; Atek et al. 2022; Castellano et al. 2022; Donnan et al. 2022; Finkelstein et al. 2022; Furtak et al. 2022; Harikane et al. 2022a; Naidu et al. 2022; Rodighiero et al. 2022; Santini et al. 2022; Topping et al. 2022; Whitler et al. 2022; Yan et al. 2022). If confirmed, the large abundance of these super-early systems is a challenge for galaxy formation models (Boylan-Kolchin 2022; Ferrara, Pallottini & Dayal 2022; Finkelstein et al. 2022; Mason, Trenti & Treu 2022).

So far, these galaxies have been identified photometrically. Spectroscopic follow-ups are necessary to confirm their detection. Such a task becomes tricky at early cosmic times because the most common emission lines used at lower redshifts shift out the observable bands or (Lyα) are severely suppressed by resonant scattering with intergalactic H I at $z > 6$. Detecting non-resonant emission lines (e.g. Hα) is the alternative strategy adopted by *JWST* NIRSpec observations.

While waiting for such data, attempts have been made to confirm the detection of $z > 10$ galaxies by using the Atacama Large sub-/Millimeter Array (ALMA) to search for fine-structure far-infrared (FIR) cooling lines, such as [O III] 88 μm and [C II] 158 μm (Bakx et al. 2022; Fujimoto et al. 2022; Kaasinen et al. 2022; Popping 2022; Yoon et al. 2022). However, these experiments have been unsuccessful so far.

Among these galaxy candidates, GHZ2 has been independently detected by several groups (Castellano et al. 2022; Donnan et al. 2022; Harikane et al. 2022a; Naidu et al. 2022) which have reported a photometric redshift $z = 11.960$–12.423. Using re-calibrated *JWST* fluxes Bakx et al. (2022) have constrained the star formation rate of GZH2 in the range ${\rm SFR} = 20^{+15}_{-14}\,{\rm M}_\odot{\rm yr}^{-1}$ and stellar mass $M_\star = 1.2^{+7.2}_{-0.4} \times 10^8\,{\rm M}_\odot$. Bakx et al. (2022) and Popping (2022) used ALMA Band 6 Director's Discretionary Time (DDT) program data to search for [O III] 88 μm line emission. Their analysis has only provided a 5σ upper limit of $\log(L_{\rm O\,III}/{\rm L}_\odot) < 1.7 \times 10^8$ (Bakx et al. 2022) for the integrated [O III] line luminosity.

Another case is GHZ1, a galaxy candidate from the *JWST* ERS program, GLASS-*JWST* (Treu et al. 2022) with a photometric redshift $z \sim 10.6$, ${\rm SFR} = 36.3^{+54.5}_{-26.8}\,{\rm M}_\odot{\rm yr}^{-1}$, and $\log(M_\star/{\rm M}_\odot) = 9.1^{+0.3}_{-0.4}$ (Santini et al. 2022). The ALMA search for [O III] 88 μm and dust continuum emission from GHZ1 was unsuccessful, albeit a marginal spectral feature was reported within 0.17 arcsec of the *JWST* position of GHZ1 (Yoon et al. 2022). The reported 5σ upper-limit of [O III] luminosity is $2.2 \times 10^8\,{\rm L}_\odot$.

For a third candidate (HD1) a tentative $z = 13.27$ was reported (Harikane et al. 2022b). To confirm this detection, ALMA Band 6 (Band 4) observations were designed to target [O III] 88 μm ([C II] 158 μm) emission (Kaasinen et al. 2022; Harikane et al. 2022b). No clear detection was found in either of the two BANDS. The 4σ upper limit for the [O III] 88 μm and [C II] 158 μm emission lines are 5.88×10^8 and $0.7 \times 10^8\,{\rm L}_\odot$, respectively (Kaasinen et al. 2022).

The last one is S5-z17-1 identified in *JWST* ERO data of Stephan's Quintet (Pontoppidan et al. 2022), which has been followed-up by ALMA Band 7 (Fujimoto et al. 2022), resulting in 5.1σ line detection at 338.726 GHz, possibly corresponding to [O III] 52 μm at $z = 16$. For this galaxy, ${\rm SFR} < 120\,{\rm M}_\odot{\rm yr}^{-1}$.

These non-detections for $z > 10$ sources discovered by *JWST* imply that either these galaxies are at lower redshifts ($z < 4$), or they are too faint to be detected with the sensitivity of the above emission line experiments (Bakx et al. 2022; Furlanetto & Mirocha 2022; Kaasinen et al. 2022).

Thus, understanding the physical nature of the possible redshift evolution of the $L_{[{\rm O\,III}]}$ − SFR relation is of utmost importance in these early stages of interpretation of *JWST* data. With this question in mind, here we analyse the [O III] 88 μm emission line from $z > 11$ simulated galaxies.

★ E-mail: mahsa.kohandel@sns.it

© 2023 The Author(s)
Published by Oxford University Press on behalf of Royal Astronomical Society

Downloaded from https://academic.oup.com/mnrasl/article/520/1/L16/6967138 by a.venera@unict.it user on 01 June 2023

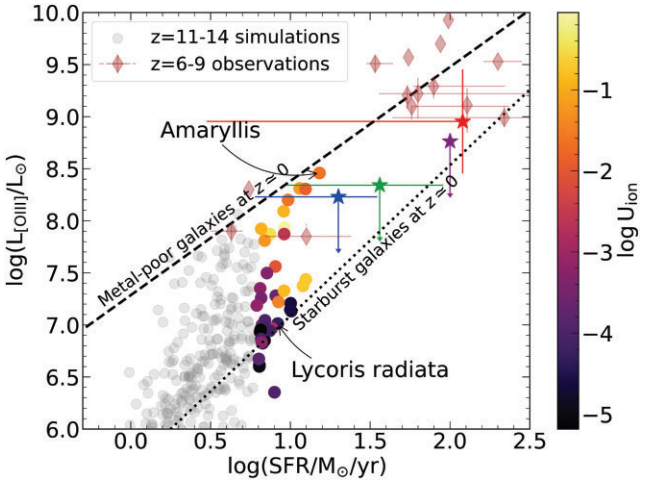

Figure 1. $L_{[\mathrm{O\,III}]}$ − SFR relation at redshift $11 \lesssim z \lesssim 14$. Circles, coloured according to the ionization parameter $U_{\rm ion}$, represent SERRA galaxies with SFR $> 6\,\mathrm{M_\odot yr^{-1}}$. Blue, green, violet, and red stars indicate ALMA upper limits for *JWST* detected super-early galaxies: GHZ2 (Bakx et al. 2022), GHZ1 (Yoon et al. 2022), HD1 (Kaasinen et al. 2022), and S5-z17-1 (Fujimoto et al. 2022), respectively. Data from $z = 6$–9 observations (Harikane et al. 2020; Witstok et al. 2022, diamonds) are shown for comparison. The $z = 0$ relations for metal-poor and starburst galaxies (De Looze et al. 2014) are shown by dashed and dotted lines, respectively.

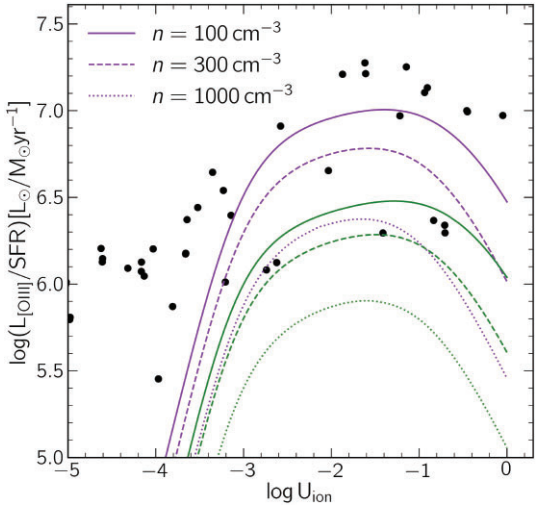

Figure 2. $L_{[\mathrm{O\,III}]}$/SFR ratio as a function of $U_{\rm ion}$ for SERRA galaxies ($z = 11$–14, black circles) along with the results from single-zone CLOUDY models (lines) for different gas density, n, as shown in the legend. The purple (green) lines correspond to $Z = 0.2\,\mathrm{Z_\odot}$ ($Z = 0.05\,\mathrm{Z_\odot}$).

2 SIMULATED SUPER-EARLY GALAXIES

SERRA is a suite of zoom-in simulations that is tailored for EoR galaxies ($z \geq 6$; Pallottini et al. 2022). In each radiation hydrodynamic simulation (Teyssier 2002; Rosdahl et al. 2013), the comoving volume is $(20\,\mathrm{Mpc\,h^{-1}})^3$ and contains ∼10–20 galaxies, whose ISM is resolved on scales of $\simeq 1.2 \times 10^4\,\mathrm{M_\odot}$ ($\simeq 30\,\mathrm{pc}$ at $z \sim 6$), i.e. the typical mass/size of molecular clouds (e.g. Federrath & Klessen 2013).

The non-equilibrium chemical network used in SERRA includes H, He, H^+, H^-, He, He^+, He^{++}, H_2, H_2^+, and e^- (Grassi et al. 2014; Pallottini et al. 2017b). Metals are produced by stars (Pallottini et al. 2017a), with solar relative abundances (Asplund et al. 2009). Line luminosities for each gas cell are computed in post-processing by using the spectral synthesis code CLOUDY (Ferland et al. 2017), accounting for the turbulent and clumpy structure of the ISM (Vallini et al. 2017, 2018), computed self-consistently from the simulation (Pallottini et al. 2019). Given a field-of-view and a line-of-sight direction, the simulated galaxies can be mapped into 3D synthetic hyperspectral data cubes (Kohandel et al. 2020) that can be directly compared with observations (Zanella et al. 2021; Rizzo et al. 2022).

In SERRA, we have 366 galaxies at $11 \lesssim z \lesssim 14$ with $M_\star \gtrsim 10^8\,\mathrm{M_\odot}$. Here, we extract a sub-sample with $6 \leq \mathrm{SFR/M_\odot yr^{-1}} \leq 35$, matching the values measured for super-early *JWST* candidates; the final sample includes 42 galaxies. These are found in dark matter halos of mass $10^{10-10.7}\,\mathrm{M_\odot}$ and are classified as *starburst* based on their position on the $\Sigma_{\rm SFR} - \Sigma_{\rm gas}$ plane[1] with $\kappa_s \sim 2$–150 (Pallottini et al. 2019).

3 [O III] EMISSION

Fig. 1 shows the position of SERRA galaxies at $z = 11$–14 on the $L_{[\mathrm{O\,III}]}$ − SFR plane, along with the super-early *JWST* observed galaxies: GHZ2 (Bakx et al. 2022), GHZ1 (Yoon et al. 2022), HD1 (Kaasinen et al. 2022), and S5-z17-1[2] (Fujimoto et al. 2022). For comparison, we show $z = 6$–9 galaxies from the literature (Harikane et al. 2020; Witstok et al. 2022), as well as the empirical relation for local metal-poor and starburst galaxies (De Looze et al. 2014).

SERRA galaxies generally fall between these two local populations, i.e. they are fainter than expected from the metal-poor relation. Moreover, although these galaxies have been selected to be in the relatively narrow star formation rate (SFR) range $6 - 35\,\mathrm{M_\odot yr^{-1}}$, their $L_{[\mathrm{O\,III}]}$ spans more than two orders of magnitude ($2.2 - 280 \times 10^6\,\mathrm{L_\odot}$). As a result, the local relation is effectively blurred as we move to the highest redshifts. This trend is also confirmed by the SERRA galaxies outside the *JWST* candidates' SFR range (grey points) which are significantly fainter than expected from the local metal-poor relation.

We note that the predicted luminosity of 3 SERRA galaxies is above the GHZ2 upper limit; hence it could have been detected. However, the detection probability critically depends on the width of the line. The full width at half-maximum (FWHM) of the [O III] line (face-on view[3]) is in the range $107 - 325\,\mathrm{km\,s^{-1}}$ with a mean of $213\,\mathrm{km\,s^{-1}}$. If we consider the most luminous galaxy in our sample ($\log(\mathrm{L_{[O\,III]}/L_\odot}) = 8.4$, FWHM$= 130\,\mathrm{km\,s^{-1}}$) located at $z = 12$, the total integration time required to detect it with ALMA at S/N=5 over the FWHM is 2.8 h on-source, which is slightly longer than the integration times (≈2 h/tuning) of all ALMA DDT programs.

4 INTERPRETATION

Based on the evidence that [O III] bright $z = 6$–9 galaxies follow local metal-poor $L_{[\mathrm{O\,III}]}$ − SFR relation (Harikane et al. 2020; Witstok et al. 2022, see points in Fig. 1), 4 different ALMA DDT experiments (Bakx et al. 2022; Fujimoto et al. 2022; Kaasinen et al. 2022; Treu et al. 2022) have been designed accordingly to detect *JWST* $z >$

[1]The burstiness parameter $\kappa_s = 10^{12}\Sigma_{\rm SFR}/\Sigma_{\rm g}^{1.4}$ is defined in equation 39 of Ferrara et al. (2019).

[2]Following Fujimoto et al. (2022), assuming that the emission feature is confirmed to be [O III] 52 μm line at $z = 16$, it can be converted to [O III] 88 μm by assuming a conversion factor of 5.

[3]Face-on view corresponds to the narrowest emission line width (Kohandel et al. 2019); thus, the estimated integration time below should be regarded as a lower limit.

Downloaded from https://academic.oup.com/mnrasl/article/520/1/L16/6967138 by a.venera@unict.it user on 01 June 2023

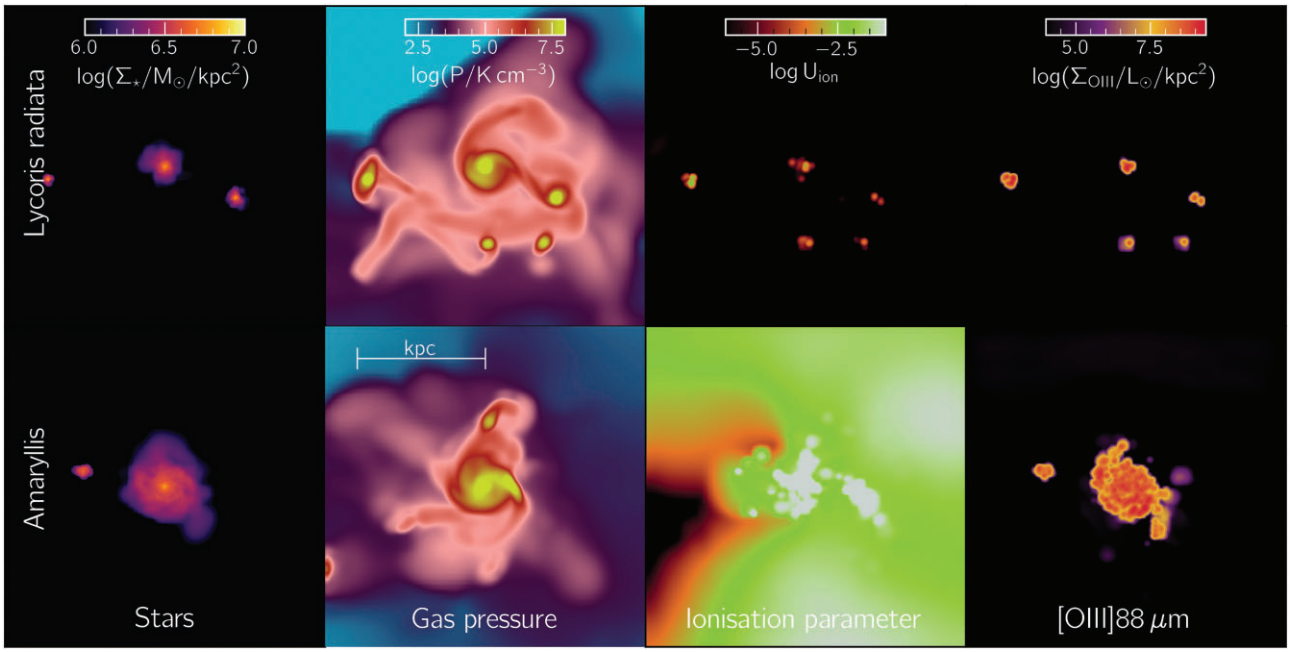

Figure 3. Stellar, gas pressure, ionization parameter, and [O III] 88 μm emission maps for two SERRA galaxies with extremely low (*Lycoris radiata*, upper panels) or high (*Amaryllis*, bottom) ionization parameters. Both systems are at $z = 11.5$ and have similar SFR and $M_\star$ (see text). *Lycoris radiata* is 20× fainter in [O III] due to its very low $U_{\rm ion}$.

10 candidates in [O III] emission. However, all failed to detect the targeted sources at the expected luminosity, providing only upper limits. The possibility exists that photometric redshifts are incorrect. Follow-up spectroscopic observations will clarify whether this is the case. Here, we work under the hypothesis that photometric redshifts are correct and non-detections are, therefore, due to the intrinsic emission properties of the galaxies.

4.1 The role of the ionization parameter

The first step to explain the unexpectedly low [O III] luminosity of super-early galaxies is to consider single-zone CLOUDY (Ferland et al. 2017) photoionization models. Similarly to Harikane et al. (2020), we assume a plane-parallel gas slab with initial gas density n, metallicity Z, and illuminated by a radiation field with ionization parameter[4] $U_{\rm ion}$. The slab is set in pressure equilibrium ($P = 10^{4.5} n$ K); the computation is stopped at a depth $A_V = 100$. The resulting $L_{\rm [O\,III]}$/SFR ratio[5] is plotted as a function of $U_{\rm ion}$ in Fig. 2 for representative models with $Z = (0.05, 0.2)\,Z_\odot$ and $n = 10^{2-3}$ cm^{-3}.

CLOUDY models predict that weak [O III] emission can be produced either by (i) low Z, (ii) high n, or (iii) low $U_{\rm ion}$. All these quantities have an impact on [O III] emission, but while n and Z show relatively small variations in the sample of simulated galaxies ($150 < n/{\rm cm}^{-3} < 1184$; $0.03 < Z/Z_\odot < 0.2$), the ionization parameter spans 5 orders of magnitude ($-5 \lesssim \log U_{\rm ion} \lesssim 0$). Hence, the strongest dependence of $L_{\rm [O\,III]}$ is on $U_{\rm ion}$, in agreement with findings by Moriwaki et al. (2018), Arata et al. (2020). The rapid drop of $L_{\rm [O\,III]}$ for $\log U_{\rm ion} \lesssim -3$ is only partially mitigated in the full RT, multiphase SERRA results (black circles). In Fig. 1, galaxies in our sample are colour-coded with $U_{\rm ion}$. Indeed, galaxies with the largest downward deviations from the local metal-poor relation have $\log U_{\rm ion} < -3$.

4.2 What determines the ionization parameter?

As galaxies in our sample, by construction, have very similar SFR values, what causes their wide ionization parameter range? Fig. 3 shows two galaxies from our sample: *Lycoris radiata* and *Amaryllis*. Shown are their stellar, gas pressure, ionization parameter, and [O III] 88 μm emission line maps. *Lycoris radiata* is a galaxy with $M_\star = 6 \times 10^8$ M$_\odot$, SFR $= 10$ M$_\odot$yr^{-1} at $z = 11.5$ and *Amaryllis* is at the same redshift with $M_\star = 6 \times 10^8$ M$_\odot$ and SFR $= 15$ M$_\odot$yr^{-1}. Although these two galaxies have similar SFR and are at the same redshift (Fig. 1), *Amaryllis* is 20× brighter in [O III] due to its higher $U_{\rm ion}$, i.e. 7×10^{-2} versus 5×10^{-5}.

The difference in $U_{\rm ion}$ is mainly driven by the compactness of H II regions. The ISM of early galaxies is highly pressurized as a result of the higher gas velocity dispersion. Fig. 3 shows that the pressure within star-forming clumps is high, $P \approx 10^{7.5}$K cm^{-3}, in both systems. As a consequence, clumps are more resistant to dispersal induced by stellar feedback, have longer lifetimes ($\gtrsim$ 10 Myr), and star formation remains embedded for a longer time (Behrens et al. 2018; Sommovigo et al. 2020). These high-density ($n \approx 10^3$ cm^{-3}) star-forming regions are characterized by $U_{\rm ion} \approx 10^{-5}$, which implies very low [O III] emission (Fig. 2). Also, ionizing photons are trapped inside the clumps and produce a super-compact H II region.

While in *Lycoris radiata* stars are almost exclusively located within high-density clumps, reflecting an earlier assembly stage in which stars are very young and still embedded, *Amaryllis* has managed to build a well-developed disc structure, within which many star clusters have dispersed their natal cloud, ionized the low-

[4] $U_{\rm ion} = n_\gamma/n$, where n_γ is the density of $h\nu > 13.6$ eV photons.
[5] The SFR is obtained from the emerging Hα luminosity using the conversion factor in Kennicutt (1998, equation 2).

Downloaded from https://academic.oup.com/mnrasl/article/520/1/L16/6967138 by a.venera@unict.it user on 01 June 2023

density ISM, and produce a high $U_{\rm ion}$. This difference can be seen from the much more extended distribution of stars with respect to clumps in *Amaryllis*. Thus, it is the ability to disperse natal clouds that ultimately determines the value of $U_{\rm ion}$ and the [O III] luminosity.

5 SUMMARY

To confirm the redshift of *JWST* detected super-early ($z > 10$) galaxies, ALMA DDT observations have been designed aiming to detect the FIR [O III] 88 μm emission line, supposing that these galaxies would follow the local metal-poor $L_{\rm [O\,III]}$ − SFR relation. Such follow-up observations have been unsuccessful so far. Non-detections can be either due to wrong photometric redshifts or to the faintness of the line in such early systems. Here, we have used the SERRA suite of simulations of $z = 11$–14 galaxies to explain such non-detections, assuming the photometric redshifts obtained by *JWST* are reliable. We find that:

(i) Galaxies with SFR similar to *JWST*-detected sources span more than two orders of magnitude in $L_{\rm [O\,III]}$; most of them are fainter than expected from the $z = 0$ metal-poor galaxies' relation.

(ii) The most luminous galaxy in our sample ($\log(L_{\rm [O\,III]}/L_\odot) = 8.4$, FWHM$= 130\,{\rm km\,s^{-1}}$) could be detected in 2.8 h on-source, which is slightly longer than the integration times (≈2 h/tuning) used by ALMA DDT programs so far.

(iii) Galaxies with the largest downward deviations from the local metal-poor relation have low ionization parameter, $\log U_{\rm ion} < -3$.

(iv) Such low $U_{\rm ion}$ values are found in galaxies that are in an early assembly stage, as most of their stars are still embedded in high-density natal clouds, and their ionizing photons are trapped in ultra-compact H II regions.

ACKNOWLEDGEMENTS

MK, AF, AP, LV, and LS acknowledge support from the ERC Advanced Grant AINTERSTELLAR H2020/740120. Generous support from the Carl Friedrich von Siemens-Forschungspreis der Alexander von Humboldt-Stiftung Research Award is kindly acknowledged (AF). We acknowledge the CINECA award under the ISCRA initiative, for the availability of high-performance computing resources and support from the Class B project SERRA HP10BPUZ8F. We gratefully acknowledge computational resources of the Center for High Performance Computing (CHPC) at SNS. We acknowledge usage of the PYTHON programming language (Van Rossum & de Boer 1991; Van Rossum & Drake 2009), Astropy (Astropy Collaboration 2013), Cython (Behnel et al. 2011), Matplotlib (Hunter 2007), NumPy (van der Walt, Colbert & Varoquaux 2011), PYNBODY (Pontzen et al. 2013), and SciPy (Virtanen et al. 2020).

DATA AVAILABILITY

The derived data generated in this research will be shared on reasonable request to the corresponding author.

REFERENCES

Adams N. J. et al., 2022, MNRAS, 518, 4755
Arata S., Yajima H., Nagamine K., Abe M., Khochfar S., 2020, MNRAS, 498, 5541
Asplund M., Grevesse N., Sauval A. J., Scott P., 2009, ARA&A, 47, 481
Astropy Collaboration, 2013, A&A, 558, A33
Atek H., Shuntov M., Furtak L. J., Richard J., Kneib J.-P., Zitrin G. M. A., Charlot H. J. M. C. L. S., 2022, MNRAS, 519, 1201
Bakx T. J. L. C. et al., 2022, MNRAS
Behnel S., Bradshaw R., Citro C., Dalcin L., Seljebotn D., Smith K., 2011, Comp. Sci. Eng., 13, 31
Behrens C., Pallottini A., Ferrara A., Gallerani S., Vallini L., 2018, MNRAS, 477, 552
Boylan-Kolchin M., 2022, preprint (arXiv:2208.01611)
Castellano M. et al., 2022, ApJ, 938, L9
De Looze I. et al., 2014, A&A, 568, A62
Donnan C. T. et al., 2022, MNRAS, 518, 6011
Federrath C., Klessen R. S., 2013, ApJ, 763, 51
Ferland G. J. et al., 2017, Rev. Mex. Astron. Astrofis., 53, 385
Ferrara A., Vallini L., Pallottini A., Gallerani S., Carniani S., Kohandel M., Decataldo D., Behrens C., 2019, MNRAS, 489, 1
Ferrara A., Pallottini A., Dayal P., 2022, preprint (arXiv:2208.00720)
Finkelstein S. L. et al., 2022, ApJ, 940, L15
Fujimoto S. et al., 2022, preprint (arXiv:2211.03896)
Furlanetto S. R., Mirocha J., 2022, preprint (arXiv:2208.12828)
Furtak L. J., Shuntov M., Atek H., Zitrin A., Richard J., Lehnert M. D., Chevallard J., 2022, preprint (arXiv:2208.05473)
Grassi T., Bovino S., Schleicher D. R. G., Prieto J., Seifried D., Simoncini E., Gianturco F. A., 2014, MNRAS, 439, 2386
Harikane Y. et al., 2020, ApJ, 896, 93
Harikane Y. et al., 2022a, preprint (arXiv:2208.01612)
Harikane Y. et al., 2022b, ApJ, 929, 1
Hunter J. D., 2007, Comp. Sci. Eng., 9, 90
Kaasinen M. et al., 2022, preprint (arXiv:2210.03754)
Kennicutt Robert C. J., 1998, ARA&A, 36, 189
Kohandel M., Pallottini A., Ferrara A., Zanella A., Behrens C., Carniani S., Gallerani S., Vallini L., 2019, MNRAS, 487, 3007
Kohandel M., Pallottini A., Ferrara A., Carniani S., Gallerani S., Vallini L., Zanella A., Behrens C., 2020, MNRAS, 499, 1250
Mason C. A., Trenti M., Treu T., 2022, preprint (arXiv:2207.14808)
Moriwaki K. et al., 2018, MNRAS, 481, L84
Naidu R. P. et al., 2022, ApJ, 940, L14
Pallottini A., Ferrara A., Gallerani S., Vallini L., Maiolino R., Salvadori S., 2017a, MNRAS, 465, 2540
Pallottini A., Ferrara A., Bovino S., Vallini L., Gallerani S., Maiolino R., Salvadori S., 2017b, MNRAS, 471, 4128
Pallottini A. et al., 2019, MNRAS, 487, 1689
Pallottini A. et al., 2022, MNRAS, 513, 5621
Pontoppidan K. M. et al., 2022, ApJ, 936, L14
Pontzen A., Rovskar R., Stinson G. S., Woods R., Reed D. M., Coles J., Quinn T. R., 2013, pynbody: Astrophysics Simulation Analysis for Python
Popping G., 2022, preprint (arXiv:2208.13072)
Rizzo F., Kohandel M., Pallottini A., Zanella A., Ferrara A., Vallini L., Toft S., 2022, A&A, 667, A5
Rodighiero G., Bisigello L., Iani E., Marasco A., Grazian A., Sinigaglia F., Cassata P., Gruppioni C., 2022, MNRASL, 518, L19
Rosdahl J., Blaizot J., Aubert D., Stranex T., Teyssier R., 2013, MNRAS, 436, 2188
Santini P. et al., 2022, preprint (arXiv:2207.11379)
Sommovigo L., Ferrara A., Pallottini A., Carniani S., Gallerani S., Decataldo D., 2020, MNRAS, 497, 956
Teyssier R., 2002, A&A, 385, 337
Topping M. W., Stark D. P., Endsley R., Plat A., Whitler L., Chen Z., Charlot S., 2022, ApJ, 941, 14
Treu T. et al., 2022, ApJ, 935, 110
Vallini L., Ferrara A., Pallottini A., Gallerani S., 2017, MNRAS, 467, 1300
Vallini L., Pallottini A., Ferrara A., Gallerani S., Sobacchi E., Behrens C., 2018, MNRAS, 473, 271
van der Walt S., Colbert S. C., Varoquaux G., 2011, Comp. Sci. Eng., 13, 22
Van Rossum G., de Boer J., 1991, CWI Q., 4, 283
Van Rossum G., Drake F. L., 2009, Python 3 Reference Manual. CreateSpace, Scotts Valley, CA
Virtanen P. et al., 2020, Nature Methods, 17, 261

Downloaded from https://academic.oup.com/mnrasl/article/520/1/L16/6967138 by a.venera@unict.it user on 01 June 2023

Whitler L., Endsley R., Stark D. P., Topping M., Chen Z., Charlot S., 2022, MNRAS, 519, 157
Witstok J. et al., 2022, MNRAS, 515, 1751
Yan H., Ma Z., Ling C., Cheng C., Huang J.-s., Zitrin A., 2022, ApJ, 942, L20
Yoon I. et al., 2022, preprint (arXiv:2210.08413)
Zanella A., Pallottini A., Ferrara A., Gallerani S., Carniani S., Kohandel M., Behrens C., 2021, MNRAS, 500, 118

This paper has been typeset from a TEX/LATEX file prepared by the author.

Downloaded from https://academic.oup.com/mnrasl/article/520/1/L16/6967138 by a.venera@unict.it user on 01 June 2023